would be released as the martian atmosphere struck the surface, a phenomenon seen earlier during perigee passes of the Earth orbital satellites Explorer C, Explorer D, and Explorer E. The mass peak at 16 includes contributions from CO_2, CO, O_2, and H_2O, in addition to a residual most probably due to O. A quantitative analysis is difficult, however, since O may be expected to react rapidly with surfaces in the instrument. It is hoped that further laboratory studies will clarify these matters, and that they might eventually permit a more quantitative estimate for the concentration of O.

The densities of NO, as shown in Fig. 2, were obtained from a detailed analysis of the peak at mass number 30. Figure 3 gives a scale representation of a typical spectrum obtained by VL1 at an altitude near 130 km. Slightly more than half of the signal at mass 30 may be attributed to $^{12}C^{18}O^+$ formed by the dissociative ionization of $^{12}C^{18}O^{16}O$. After correction for $^{12}C^{18}O^+$ from both CO_2 and CO, there remains a component whose magnitude significantly exceeds the noise level of the amplifier. This component is most reasonably attributed to NO, and it is seen in all spectra for which the peak at mass 30 exceeds the amplifier noise background. The data indicate a mixing ratio for NO relative to CO_2 of approximately 10^{-4}. The density of NO in the upper atmosphere of Mars is thus significantly higher than the density of NO at comparable levels of Earth's atmosphere.

It is clear from even a casual inspection of the data in Fig. 2 that the martian atmosphere must be mixed to heights greater than 130 km. This observation implies an eddy diffusion coefficient of at least 5×10^7 cm^2 sec^{-1}. One would expect a density for N_2 of about 5×10^7 cm^{-3} at 190 km in VL1, or about 10^8 cm^{-3} at 160 km in VL2, if diffusive separation should occur above 130 km. The measured densities at these altitudes are only 2×10^7 cm^{-3} and 4×10^7 cm^{-3}, respectively. The densities as measured for CO are also consistent with the assumption of rapid vertical mixing, as discussed elsewhere (*9*).

The upper atmospheric mass spectrometers on both VL1 and VL2 used Mattauch-Herzog geometry (*10*), which allowed for simultaneous collection of ions with different masses. Two collectors were used to measure ions differing in mass by approximately a factor of 7 (*7*). The heavy collector was sensitive to the mass range 7 to 49 atomic mass units (amu), whereas the light collector recorded ions in the range 1 to 7 amu. Because of weight restrictions imposed at an early stage of the project, we were obliged to use electrometer amplifiers rather than electron multipliers. The background fluctuations of these amplifiers were in the range (1 to 5) $\times 10^{-14}$ amp. The instrumental sensitivity on Viking was therefore less than that for similar instruments flown on sounding rockets and terrestrial satellites, by about a factor of 10^3. The low-mass spectra are currently being analyzed: preliminary results suggest upper limits for the mixing ratios of H_2 and He relative to CO_2 of about 10^{-4}.

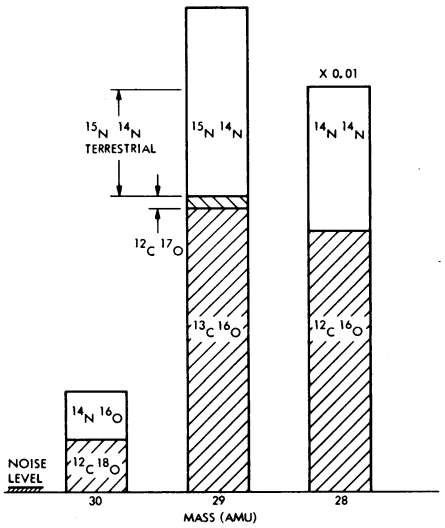

Fig. 3. Block diagram representing to scale the relative heights for the mass peaks at 30, 29, and 28 amu in a spectral scan obtained near an altitude of 130 km during the descent of VL1. The diagram shows the contribution of CO^+ (from the fragment due to the dissociation of CO_2 in the ion source and from ambient CO) to the several peaks. The remainder, in the case of the peaks at mass 29 and 28, is attributed to ambient N_2. The excess peak at mass 30 is attributed to ambient NO. The diagram also illustrates that both the excess peak at mass 30 and the excess peak at mass 29 (beyond that expected if the nitrogen has a terrestrial isotopic composition) are well above the noise level of the amplifier which measured the ion currents.

A. O. NIER

School of Physics and Astronomy, University of Minnesota, Minneapolis

M. B. MCELROY

Center for Earth and Planetary Physics, Harvard University, Cambridge, Massachusetts 02138

References and Notes

1. A. O. Nier, W. B. Hanson, A. Seiff, M. B. McElroy, N. W. Spencer, R. J. Duckett, T. C. D. Knight, W. S. Cook, *Science* **193**, 786 (1976). A typographical error appears in line 11, column 1, p. 787. The sentence should read "Peaks at masses 18 and 17 are. . . ."
2. A. O. Nier, M. B. McElroy, Y. L. Yung, *ibid.* **194**, 68 (1976).
3. K. Biemann, T. Owen, D. R. Rushneck, A. L. LaFleur, D. W. Howarth, *ibid.*, p. 76.
4. M. B. McElroy, Y. L. Yung, A. O. Nier, *ibid.*, p. 70.
5. M. B. McElroy, *ibid.* **175**, 443 (1972).
6. F. D. Colegrove, W. B. Hanson, F. S. Johnson, *J. Geophys. Res.* **70**, 4931 (1965); R. S. Lindzen, *Mesospheric Models and Related Experiments*, G. Giocco, Ed. (Reidel, Dordrecht, Netherlands, 1971), p. 120.
7. A. O. Nier and J. L. Hayden, *Int. J. Mass Spectrom. Ion Phys.* **6**, 339 (1971).
8. A. O. Nier, J. H. Hoffman, C. Y. Johnson, J. C. Holmes, *J. Geophys. Res.* **69**, 979 (1964); A. O. Nier, W. E. Potter, D. R. Hickman, K. Mauersberger, *Radio Sci.* **8**, 271 (1973); J. B. French, N. M. Reid, A. O. Nier, J. L. Hayden, *CASI Trans.* **5**, 77 (1972); J. L. Hayden, A. O. Nier, J. B. French, N. M. Reid, R. J. Duckett, *Int. J. Mass Spectrom. Ion Phys.* **15**, 37 (1974).
9. M. B. McElroy, T. Y. Kong, Y. L. Yung, A. O. Nier, *Science* **194**, 1295 (1976).
10. J. Mattauch and R. Herzog, *Z. Phys.* **89**, 786 (1934).
11. Work at the University of Minnesota and at Harvard University was supported under NASA contracts NAS-1-9697 and NAS-1-10492, respectively. A.O.N. is indebted to M. Wade and W. Johnson for help in the computations.

12 November 1976

Structure of Mars' Atmosphere up to 100 Kilometers from the Entry Measurements of Viking 2

Abstract. *The Viking 2 entry science data on the structure of Mars' atmosphere up to 100 kilometers define a morning atmosphere with an isothermal region near the surface; a surface pressure 10 percent greater than that recorded simultaneously at the Viking 1 site, which implies a landing site elevation lower by 2.7 kilometers than the reference ellipsoid; and a thermal structure to 100 kilometers at least qualitatively consistent with pre-Viking modeling of thermal tides. The temperature profile exhibits waves whose amplitude grows with altitude, to ~ 25°K at 90 kilometers. These waves are believed to be a consequence of layered vertical oscillations and associated heating and cooling by compression and expansion, excited by the daily thermal cycling of the planet surface. As is necessary for gravity wave propagation, the atmosphere is stable against convection, except possibly in some very local regions. Temperature is everywhere appreciably above the carbon dioxide condensation boundary at both landing sites, precluding the occurrence of carbon dioxide hazes in northern summer at latitudes to at least 50°N. Thus, ground level mists seen in these latitudes would appear to be condensed water vapor.*

The second Viking lander entered the atmosphere of Mars on 3 September 1976 at about 3:49 p.m. Pacific Daylight Time (P.D.T.), and landed at 3:58:20 p.m. P.D.T. in Utopia Planitia at 47.66°N latitude and 225.78°W longitude at 9:06

a.m. Mars local time. During entry and descent, measurements were made to define the structure of the atmosphere below about 120 km, as on Viking 1 (*1*). Real-time transmission of the entry data to the earth, by relay through the orbiter, was prevented by problems with the attitude stabilization of the orbiter during this period. The data were recorded on tape recorders, however, on both the orbiter and the lander, and were transmitted to the earth from the orbiter record almost exactly 24 hours later. The results presented here are based on analysis of the first orbiter replay.

We present a preliminary analysis, which does not include all the corrections and refinements that will ultimately be applied. The primary corrections omitted here are corrections for effects due to atmospheric winds, final corrections for terrain variations under the flight path, and small corrections for such instrument effects as response lag and radiative input. [The latter are known to be small from previous studies (*2*).] We believe that the results presented here substantially represent the atmosphere sensed by Viking 2.

The instruments and techniques applied to obtain and analyze the data have been described (*2*, *3*). The primary instrument for altitudes above 25 km was a three-axis set of accelerometers, accurate to within 0.02 percent of reading. Two sets of pressure and temperature sensors were provided, one for the entry phase before heat shield jettison and parachute deployment (at nominally 6 km in altitude) and the other for the parachute descent. Altitude data taken by the lander radar altimeter below about 130 km were also invaluable.

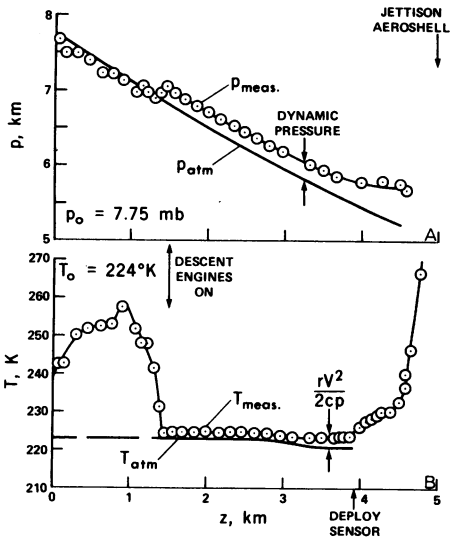

Fig. 1. Measurements of temperature and pressure taken during parachute descent. The interval of good data is constrained by descent engine firing at 1.5 km and (for temperature) by lander leg deployment at 3.9 km.

Table 1. Surface elevations at the Viking 2 landing site indicated by measurements of the planet's radius after landing.

	Radius (km)		Landing site elevation $b - a$ (km)
	Smooth ellipsoid (a)	Measured (b)	
Topographic	3385.0 ± 0.7 (*14*)	3381.4 ± 1.3 (*15*)	−3.6 ± 1.5
Gravitational	3384.3 ± 0.7 (*14*)	3381.5 ± 0.6 (*16*)	−2.8 ± 0.9

The first data interpreted after touchdown were the temperature and pressure measurements during parachute descent, shown in Fig. 1. Significant atmospheric temperature data were obtained by the sensor mounted on footpad 2, from the time of leg deployment at 3.9 km to retrorocket firing at 1.5 km. The dynamic corrections shown applied to the measured temperatures, about 1.5°K, are required for descent velocities on the parachute between 50 and 60 m/sec, as measured by the Doppler radar during descent. The atmosphere is seen to be isothermal from 1.5 to 4 km, with a lapse rate of at most 1.3°K/km above 2.5 km. This is in contrast to the lapse rate of 3.7°K/km reported for Viking 1 (*1*).

This difference between the near-surface temperature profiles is a diurnal effect, which has been discussed theoretically (*4*). In the morning profile of Viking 2, the near-surface atmosphere has been cooled overnight by radiation. In the late afternoon profile of Viking 1, it has been warmed by midday radiation from the surface.

The atmospheric pressure profile defined by parachute-phase sensing from 1.5 to 4.5 km and its correction for descent velocity are shown in Fig. 1A. Corrections range from about 0.2 mbar at the lower altitudes to about 0.5 mbar at 4.5 km. The atmospheric pressure curve extrapolates to 7.75 mbar at the surface (*5*). Simultaneously at the Viking 1 site on that date, the pressure was 6.98 mbar, and the mean for that sol was 7.13 mbar (*6*). This indicates that the landing site of Viking 2 was 0.96 to 1.20 km below that of Viking 1 (*7*). The "6.1-mbar reference surface" is 2.7 km above the Viking 2 landing site (*8*).

Low surface elevations at the Viking 2 landing site were also indicated by planet radius measurements after landing, by means of radio tracking and measured acceleration due to gravity (3.7307 m/sec^2), as shown in Table 1. Elevation measured at the Viking 1 site was − 1.7 to − 2.0 km. Thus, the elevations measured independently are consistent with the measured pressures, and the elevation difference with the measured pressure difference.

The profile of density for the altitude range to 100 km defined by Viking 2 (primarily by the accelerometers) is shown in Fig. 2. (The upper altitude limit will ultimately extend to about 125 km.) Densities determined independently from stagnation pressure measurements are included as circular symbols, and agree well with those defined by the deceleration. The curve joins smoothly with parachute descent data based on temperature and pressure with an assumed composition of 0.947 CO_2, 0.035 N_2, 0.015 Ar, and 0.003 O_2 (see below). The computed surface density is 0.0180 kg/m^3. Curvature and waviness in the profile signify a nonisothermal atmosphere.

Integration of the density distribution under the assumption of hydrostatic equilibrium yields the pressure profile with altitude given in Fig. 3. The pressure profile is less wavy than the density profile, and again goes very smoothly into the directly sensed pressures in the parachute descent. Altitudes are measured above the landing site, throughout.

From the densities and pressures in Figs. 2 and 3 and the equation of state, the temperature profile in Fig. 4 is calculated. An atmospheric mean molecular weight of 43.34 was assumed, based on

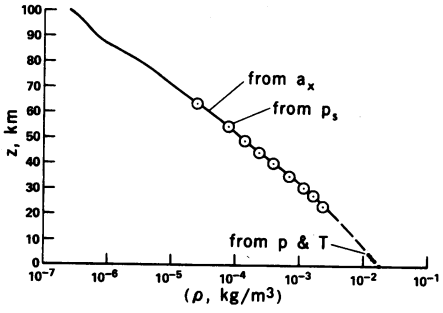

Fig. 2. Profile of atmospheric density to 100 km in altitude. For the acceleration data reduction, laboratory drag coefficients in a CO_2 atmosphere at simulated velocities and Reynolds numbers are used; these are believed accurate to within 1 percent below about 85 km (*2*). The stagnation pressure analysis is based on the same velocity history, but is otherwise independent. The accelerometer data will, when analysis is complete, fill the gap shown from about 5 to 25 km.

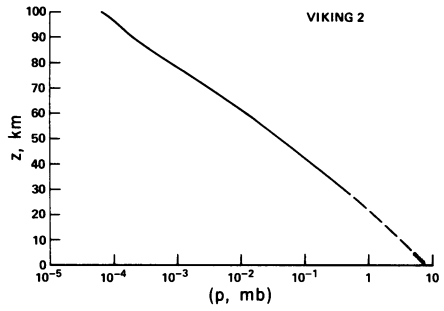

Fig. 3. Pressure profile of Mars atmosphere to 100 km. Above 90 km, the uncertainty in temperature at the experiment threshold also affects pressure by perhaps ± 10 percent at 100 km, diminishing to ± 1 percent at 80 km.

data given by the upper atmospheric (*1*) and landed (*9*) mass spectrometers, used to select the composition given above.

The temperature profile is characterized by a subadiabatic lapse rate of 1.8°K/km between 5 and 19 km, above which there is a temperature oscillation about the mean. This wave appears to confirm the presence of the diurnal thermal tide modeled for martian atmospheric conditions by Zurek (*10*). Figure 5, reproduced from Zurek (*10*), shows the correspondence. Although none of the cases presented matches the Viking 2 latitude and season, the similarity in the wave structure is evident. More detailed comparisons should indicate the changes required in the model to achieve quantitative correspondence.

Vertical wavelengths (altitude differences from peak to peak) range from 17 to 23 km in the data. Theoretical wavelengths range from 22 to 24 km. The physical interpretation of the temperature maxima and minima is that the fluid, oscillating vertically in the thermally driven gravity waves, is alternately heated by compression and cooled by expansion. The oscillations occur in several layers, whose thickness is the apparent wavelength in temperature, with phase alternation between layers, while the gravity wave propagation has a major horizontal component. Radiative transfer acts to reduce the temperature differences vertically. To generate the observed temperature amplitudes adiabatically at the six peaks below 80 km requires compression ratios from 1.26 to 0.80 in pure CO_2. For these six peaks, the vertical motion amplitudes need be only 0.6 to 2.1 km. The uppermost peak, if read to a mean temperature of 134°K, requires a motion amplitude of 6.6 km.

The wave structure was also seen in the Viking 1 preliminary temperature profile (*1*) and in the profiles derived from the occultation of ε Geminorum (*11*). The latter are phase-shifted relative to the Viking 2 profile—there is a maximum in the occultation immersion profile at 80 km and a minimum at 70 km—a result, no doubt, of the times of day at the occultation sites, which were not stated. The further analysis of the Viking 1 thermal structure has not altered its basic form, but has extended it in altitude and somewhat increased its regularity.

As required to support gravity waves, the Viking 2 temperature profile is convectively stable, probably so even in the regions of decreasing temperature above the wave peaks. The upward propagation of the diurnal surface heating therefore takes place predominantly by radiation, and hence depends quantitatively on the dust content of the atmosphere.

The temperatures, as for Viking 1, are everywhere well above the CO_2 condensation boundary. Since this is a morning profile, it appears unlikely that CO_2 hazes form at latitudes to 50°N in northern summer. The minimum overnight ground temperature of 180°K also supports this conclusion (*12*). Water ice clouds would form, of course, given sufficient water vapor, and where morning mists are seen in these summer latitudes it is presumed that they are water.

The two curves shown above 80 km in Fig. 4 are for two assumed initial temperatures at 100 km. These initial temperatures were selected from an analysis of the data to 110 km, in which starting temperatures from 100° to 170°K converge to 135° ± 5°K at 100 km. All of these cases converge within ± 1°K at 80 km. The

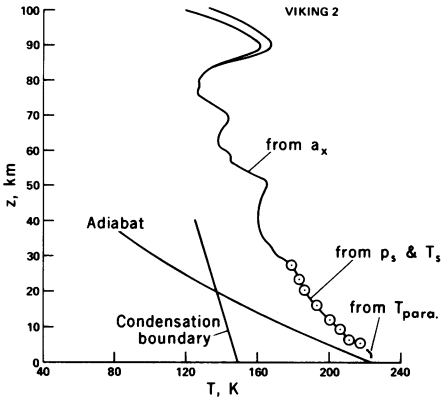

Fig. 4. Temperature structure of the atmosphere seen by Viking 2. Above 29 km, temperature is derived from acceleration data; below that, from measured temperatures and pressures. The three sets of independent measurements, including those on the parachute, are highly self-consistent. The limited isothermal region near the ground gives way to a region of subadiabatic lapse with what is apparently the diurnal thermal wave superimposed.

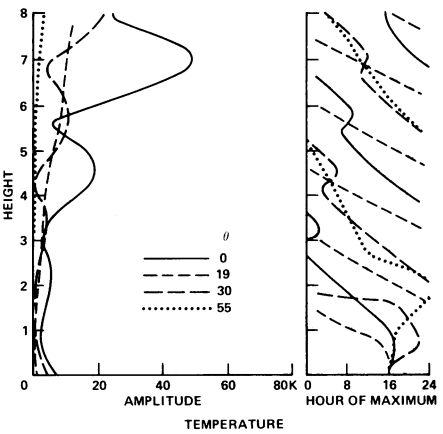

Fig. 5. Vertical profiles of diurnal temperature amplitude and phase, after Zurek (*10*). The cases presented here are for northern latitudes at southern summer solstice on a smooth planet at the prime meridian. Height is in units of 10 km. The time dependence of the temperature is sinusoidal (in the model). The amplitude typically varies periodically with altitude, but in one case (θ = 19° latitude) does not.

profiles shown are also consistent with temperature data obtained by Nier (*13*) from the entry science mass spectrometer, at altitudes above 120 km. There will be further efforts to improve analysis of the threshold region, possibly by joint consideration of densities from the accelerometer and the mass spectrometer to determine pressure at 120 km without assumption.

A computation was performed to test the sensitivity of the temperature profile to uncertainties in the lander drag coefficient and angle of attack at the highest altitudes (above 90 km), for which the Reynolds numbers are very low and the aerodynamics not as well defined. An angle of attack of 11.2° was, in this test calculation, imposed throughout the region above 60 km, instead of permitting angle of attack to be defined by the ratio of lateral to axial acceleration, and the drag coefficient corresponding to 11.2° was imposed, instead of allowing the computer program to select drag coefficient from tables based on angle of attack. Changes in drag coefficient up to 8 percent were thus introduced. Because of compensating effects, the changes in temperature profile were small, nowhere greater than 2°K. Hence, current uncertainties in the aerodynamics at extremely high altitudes apparently do not affect the results presented.

ALVIN SEIFF
DONN B. KIRK
Space Science Division,
NASA Ames Research Center,
Moffett Field, California 94035

References and Notes

1. A. O. Nier, W. B. Hanson, A. Seiff, M. B. McElroy, N. W. Spencer, R. J. Duckett, T. C. D. Knight, W. S. Cook, *Science* **193**, 786 (1976).
2. A. Seiff, *Space Sci. Instrum.*, in press.
3. A. O. Nier, W. B. Hanson, M. B. McElroy, A. Seiff, N. W. Spencer, *Icarus* **16**, 74 (1972).
4. P. Gierasch and R. Goody, *Planet. Space Sci.* **16**, 615 (1968).
5. The fact that the atmospheric pressure curve passes near the measured values during descent engine operation is probably fortuitous.
6. Viking Meteorology Team, personal communication.
7. An order of magnitude estimate shows that the pressure difference between the sites cannot be accounted for by dynamics. Pressure differences due to measured wind velocities are on the order of 10^{-3} mbar.
8. It is now clear that this reference level cannot be identified with a specified atmospheric pressure, since pressure varies seasonally [S. L. Hess *et al.*, *Science* **194**, 78 (1976)]. By chance, pressure at the reference ellipsoid was 6.14 mbar (from Viking 1 data) on 3 September 1976.
9. T. Owen and K. Biemann, *Science* **193**, 803 (1976).
10. R. W. Zurek, *J. Atmos. Sci.* **33**, 321 (1976).
11. J. L. Elliot, R. G. French, E. Dunham, P. J. Gierasch, J. Veverka, C. Church, C. Sagan, *Science*, in press.
12. H. H. Kieffer, S. C. Chase, Jr., D. D. Miner, F. D. Palluconi, G. Münch, G. Neugebauer, T. Z. Martin, *ibid.* **193**, 780 (1976).
13. A. O. Nier, personal communication.
14. E. J. Christensen, *J. Geophys. Res.* **80**, 2909 (1975).
15. Radio tracking radius (personal communication from E. Euler of the Viking Flight Team).
16. Radius from measured acceleration due to gravity (personal communication from E. J. Christensen).

17. The authors extend their appreciation to S. Cook of the Viking Entry Science team and to E. Euler, F. Hopper, R. Dupree, and others of the Viking Flight Team who provided invaluable support. Thanks also are due to many colleagues at Ames Research Center, in particular S. Rogallo for computer programming support and to S. C. Sommer for support during the mission operations period. The authors are further indebted to C. B. Leovy for helpful discussions on the thermal tidal processes.

18 October 1976

Viking Magnetic Properties Investigation: Further Results

Abstract. *The amounts of magnetic particles held on the reference test chart and backhoe magnets on lander 2 and lander 1 are comparable, indicating the presence of an estimated 3 to 7 percent by weight of relatively pure, strongly magnetic particles in the soil at the lander 2 sampling site. Preliminary spectrophotometric analysis of the material held on the backhoe magnets on lander 1 indicates that its reflectance characteristics are indistinguishable from material within a sampling trench with which it has been compared. The material on the RTC magnet shows a different spectrum, but it is suspected that the difference is the result of a reflectance contribution from the magnesium metal covering on the magnet. It is argued that the results indicate the presence, now or originally, of magnetite, which may be titaniferous.*

The aim of the Viking magnetic properties investigation (*1*) is to estimate the abundance and composition of magnetic minerals in the martian surface material at the Viking landing sites. Two magnet arrays in the surface sampler backhoe enter the surface material during sample acquisition and attract and hold any magnetic particles present. Another array mounted on one of the imaging reference test charts (RTC) on top of each lander attracts magnetic particles already in, or raised into, the Martian atmosphere.

Details of the magnet arrays have been given by Hargraves *et al.* (*2*). Briefly, each array consists of a cylindrical magnet surrounded by, and separated from, a ring magnet. The overall dimensions of each array are 1.8 cm diameter and 0.3 cm thick, and the central and ring magnets are oppositely magnetized along their axes. Two arrays are placed in the backhoe in such a way that their surfaces are respectively 0.5 mm and 3.0 mm below the backhoe surface on one side and 3.0 mm and 0.5 mm below on the other; thus, at each face of the backhoe there are two levels of attractive force, in the approximate ratio of 12 : 1. Images of the backhoe are periodically taken by the lander cameras, the back face directly and the front by way of a 4× magnifying mirror. The RTC magnet is a single array equivalent to a strong backhoe array.

Results from Viking 1. Results from Viking 1 (VL1), based on images received up to sol 34, have already been described (*2*) and are summarized here.

After initially attracting some particles out of the dust cloud raised by the terminal descent engines during the final stages of the landing, the magnet on the RTC attracted considerably more material during the mission, indicated by a well-defined bull's-eye pattern of particles over the magnet array. The chief source of this material is believed to be dust raised by surface sampling activity and subsequent distribution of the soil samples to the three analytical experiments. There may also be a contribution from magnetic particles attracted from the martian atmosphere.

The backhoe magnets attracted a considerable quantity of relatively low albedo magnetic particles from the soil during surface sampling activity, including one or two small fragments 2 to 3 mm across. The existence of well-defined bull's-eye patterns of similar extent on both strong and weak magnets indicated the presence in the soil of a strongly magnetic, relatively pure mineral. This was considered most likely to be magnetite, and by comparison with laboratory tests on terrestrial materials its abundance was estimated as 3 to 7 percent by weight.

On sol 40, a high resolution, direct view image of the backhoe was received, after a cumulative total of 13 insertions into the surface. This image indicates that slightly more material was held on sol 40 than on sol 28, and that some millimeter-sized fragments were still adhering on sol 40.

On sol 41, further images of the backhoe were received that were taken during a special sequence in which insertion of the backhoe into the surface was followed by imaging, by way of the magnifying mirror, the material held on the front of the backhoe both before and after vibration. Considerably more material was held on the magnets before than after vibration of the collector head, indicating that much non- or weakly magnetic material entrained with the strongly magnetic particles was purged by this vibration.

A list of images of the RTC and backhoe magnets received since sol 34 is given in Table 1. [For a list of previous images received, see (*2*).]

Results from Viking 2: The RTC magnet. A low resolution image made in the survey mode on Viking 2 (VL2) on sol 0, in which no clear bull's-eye pattern can be discerned, and a high resolution image on sol 6 were received before any sampling activity had occurred (Fig. 1a). In the sol 6 image there was significantly more material on the magnet than was observed on the Viking 1 magnet at the nearest corresponding time (sol 3). This could have been the result of a relatively larger or denser dust cloud which might have been raised during the landing of VL2 because of an extra burn of the terminal descent engines just before touchdown. It is believed that the material was not seen in the sol 0 image of the magnet because of its small size and the lack of contrast. A comparison of the material held on the RTC magnets on sol 15 (VL1) and sol 13 (VL2) shows somewhat less material held on the latter than the former. On both landers there was sampling activity on sol 8, but because of an anomaly on the surface sampler only one delivery had occurred on VL2 as opposed to four on VL1. This difference probably explains the above observations.

A further comparison of the RTC magnets on the two landers can be made for sols 31 (VL1) and 33 (VL2). After a simi-